Merging Open-Tubular and Packed Bed Liquid Chromatography

ARTICLE *in* ANALYTICAL CHEMISTRY · JUNE 2015

Impact Factor: 5.64 · DOI: 10.1021/acs.analchem.5b01579 · Source: PubMed

4 AUTHORS, INCLUDING:

Gert Desmet
Vrije Universiteit Brussel
254 PUBLICATIONS **3,740** CITATIONS
SEE PROFILE

Heidi Ottevaere
Vrije Universiteit Brussel
185 PUBLICATIONS **1,152** CITATIONS
SEE PROFILE

Wim De Malsche
Vrije Universiteit Brussel
81 PUBLICATIONS **551** CITATIONS
SEE PROFILE

analytical chemistry

Article

pubs.acs.org/ac

Merging Open-Tubular and Packed Bed Liquid Chromatography

Gert Desmet,[†] Manly Callewaert,[†,‡] Heidi Ottevaere,[‡] and Wim De Malsche*[,†]

[†]Department of Chemical Engineering, Vrije Universiteit Brussel, Pleinlaan 2, 1050 Brussels, Belgium

[‡]B-PHOT, Department of Applied Physics, Vrije Universiteit Brussel, Pleinlaan 2, 1050 Brussels, Belgium

Supporting Information

ABSTRACT: Experimental and theoretical proof is provided for the fact that a microfabricated packed bed column, which is uniformly filled with radially elongated pillars (REPs), can produce the same separation performance as nonpacked, open-tubular columns. These are generally recognized as the best possible chromatographic column format, offering the highest conceivable separation speed and efficiency. It is also demonstrated both experimentally and theoretically that, as long as pressure is not a limiting factor, the REP column format can even outperform the open-tubular column format, with significant gains in either speed or efficiency proportional to the tortuosity, τ, of the bed. Conducting chromatographic experiments on 4 cm long micromachined packed bed columns filled with radially elongated pillars, separation efficiencies corresponding to N = 160 000 theoretical plates (unretained analytes) and N = 70 000 theoretical plates were achieved, despite the relatively large interpillar distance (2.5 μm).

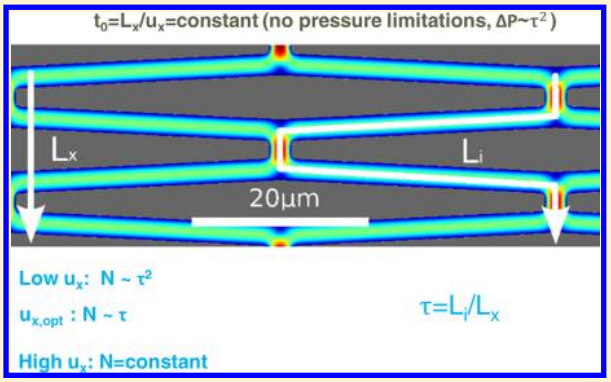

In terms of the number of resolvable components, chromatography is maybe one of the most powerful separation techniques. Capable of turning minute retention equilibrium differences into a distinct difference in migration speed through a packed bed or open-tubular column, chromatography can resolve highly complex samples composed of hundreds or thousands of components into their individual substituents.[1−7] Whereas the open-tubular column format intrinsically offers a superior speed and efficiency and has become the industry standard in gas chromatography, the vast majority of liquid-phase chromatography separations is still conducted in packed bed columns, packed with porous or partially porous spheres with a diameter in the order of 1.5 to 5 μm or with so-called monolithic columns.[1] Open-tubular column (OTC) and packed bed columns are generally considered as totally different formats, with even different laws to describe their efficiency.[8,9] In the 1980s, many research efforts were undertaken to put OTCs to work for LC.[8] With the dramatic increase in detection sensitivity of MS, there is a revived interest in OTC for liquid-phase chromatography,[10,11] including the move to extreme degrees of miniaturization where chromatographic separations in the core of a single nanotube have been demonstrated.[12]

In 2007, our group presented the first successful chromatographic separations in so-called micropillar array columns under pressure-driven flow conditions,[13] later followed by others.[14,15] Originally proposed by He et al. in 1998 for use under electrically driven flow conditions, a pillar array column can be considered as the 2D equivalent of the sphere packing in a packed bed column. As they are produced using micromachining technology in silicon or glass, pillar array columns offer the clear advantage that the pillars can be arranged in a perfectly ordered and reproducible way.[16]

In the present study, we propose a sound theoretical basis for the separation speed limits of pillar array columns where the pillars are not cylindrical (as is the obvious 2D equivalent to packed bed of spheres, cf. Figure 1a) but have a radially stretched, diamond shape (Figure 1b). Very recently, we found

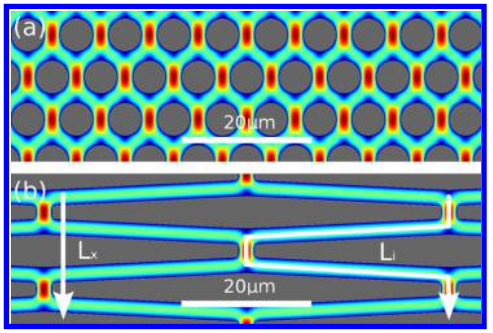

Figure 1. Top view of pillar arrangement and velocity field of (a) a conventional cylindrical pillar array column and (b) a radially elongated pillar (REP) column with AR = 9. White arrow L_x indicates the net direction of flow; white arrow L_i indicates the direction of flow along the tortuous path followed by the liquid.

Received: April 27, 2015
Accepted: June 15, 2015

DOI: 10.1021/acs.analchem.5b01579
Anal. Chem. XXXX, XXX, XXX−XXX

that such radially elongated pillar (REP) columns lead to a significant reduction of the minimal plate height, which is the main separation efficiency indicator of chromatographic systems.[17] A drawback of these REP columns however was that the velocity at which this minimal plate height is reached also decreased. Another drawback is that the larger flow obstruction leads to a larger pressure drop.

To investigate whether the observed advantage of a smaller minimal plate height can outweigh these disadvantages, a new set of REPs columns has been produced, covering a broader range of pillar aspect ratios (ARs) and with a higher machining precision, using a fully optimized Bosch etching program to minimize the vertical taper of the cross-section of the flow-through pores. This high accuracy was needed to omit any bias from additional band broadening sources (taper of pillar cross-section, uneven etch depths across column) to accurately verify a hypothesis we developed when studying the velocity field prevailing in REP columns (cf. Figure 1b). This hypothesis is that the intrinsic band broadening experienced by the fluid in the tortuous paths meandering between the REPs is identical to that experienced in an open-tubular column (OTC) with the same, flat-rectangular cross-section as the through-pores in the REP columns (dimensions $d \times h$, where d is the distance between the pillars and h is the height of the pillars). The only difference between the flow in a straight OTC and that in a large aspect ratio REP column would be the presence of turns and connection points in the case of the latter, but it can be speculated that these only make up a small fraction of the total trajectory and can hence be neglected (at least for the most elongated pillars).

EXPERIMENTAL SECTION

Microfabrication, Channel Design, and Retentive Layer Coating. Four types of pillar-array columns (always 18 μm deep, 40 mm long, 1 mm wide, and with an interpillar distance of 2.5 μm) with different aspect ratios (AR = 9, 12, 15, and 20) were fabricated. The axial dimension of the structure was 5 μm in all cases; the lateral dimension was, respectively, 45, 60, 75, and 100 μm for AR 9, 12, 15, and 20. They were patterned using mid-UV photolithography (photoresist, Olin 907-12), followed by a dry deep reactive ion etching (DRIE) step (Adixen AMS100DE, Alcatel Vacuum Technology, Culemborg, The Netherlands) to etch the 200 nm thick SiO_2 hard mask underneath. Next, the supply channels were defined by mid-UV lithography through a Chrome coated quartz plate. Etching of the SiO_2 layer was performed by a Bosch-type deep-reactive-ion etching step (Adixen AMS100SE). After removal of the photoresist by oxygen plasma and nitric acid, the pillars were subsequently defined in the SiO_2 mask (and also the already defined and partly etched capillary groove) and were finally DRIE etched to a depth of 18 μm deep.[18] The patterned Si device was then sealed with a Borofloat wafer (thickness 0.5 mm) by anodic bonding (EVG EV-501, EV Group Inc., Schaerding, Austria). The chip was subsequently diced (100 μm deep) from the top and bottom and then cleaved such that the grooves fitting the connection capillaries (108 μm OD and 40 μm ID) become accessible. Finally, the connection capillaries were inserted and sealed in these grooves using (epoxy) glue. Subsequently, a chlorodimethyloctylsilane (C8) coating was applied on the silicon pillars (which are covered with a thin native layer of SiO_2) by means of the following liquid-phase coating procedure. The channels were first flushed with methanol (1 d) and anhydrous toluene (1 d). Next, a solution of C8 in anhydrous toluene was pumped through the channel (3 d, room temperature). The coating procedure was completed by flushing the channels with anhydrous toluene (1 d) and methanol (1 d).

Sample and Liquids. The dyes used in the separation experiments, Coumarin C440 (CAS no. 26093-31-2, Sigma-Aldrich, Belgium), C450 (CAS no. 26078-25-1), C460 (CAS no. 91-44-1), and C480 (CAS no. 41267-76-9), were dissolved in filtered methanol (1 mM) and subsequently further diluted with filtered demi-water and methanol (Sigma−Aldrich, Belgium) mixtures (0.40 mM, 0.50 mM, 0.17 mM, and 0.20 mM for C480, C460, C450, and C440, respectively).

Injection and Detection. The sample injection was performed using an on-chip injection box with two inlets and outlets and controlled via an automated valve system, controlled with an in-house written C++ program.[18] Typically, 0.1 mm wide bands are injected, corresponding to some 1.4 nL. First, the injection box is filled with sample by using inflow and outflow channels, while keeping the mobile phase inlet and outlet of the column closed. Next, the valves are switched to enable a mobile phase flow into the column. The sample and mobile phase flow were generated using two pressurized nitrogen vessels. During the sample injection step, the valve system closes the inlet and the outlet of the mobile phase circuit. The inlet and the outlet of the sample injection circuit are then diverted to a high flow resistance capillary during the subsequent sample separation, allowing for a small leakage flow thus avoiding tailing. A mercury vapor lamp was used to excite the fluorescent dye in the UV. An air-cooled, high speed 14bit CCD fluorescence camera (Hamamatsu Photonics K.K., Japan) was used to visualize the sample bands.

Plate Height Measurement. The sample band intensity profiles were analyzed using Simple PCI image analysis software. On-column concentration profiles were obtained by adding all fluorescence intensity values recorded on the same transversal row of pixels. The resulting axial concentration distribution was subsequently fitted with a Gaussian function with Matlab to determine its spatial variance σ_x^2. Local H values were subsequently obtained as $(\sigma_{x,2}^2 - \sigma_{x,1}^2)/\Delta x$, with $\sigma_{x,2}^2$ and $\sigma_{x,1}^2$ being the variance of the band at positions 1 and 2 and Δx being the distance between both positions.

Velocity Field Simulations. To illustrate how the velocity depends on the geometry and how the tortuosity (τ) values, defined further in eq 1, vary with the aspect ratio of the pillars (see Table 1 for results), the velocity field in the REP columns has been calculated using Comsol software (version 4.3). The flow domains were gridded using triangular cells with a density of about 10^4 cells per square micrometer (the shortest diagonal of pillars in Figure 1 is 5 μm). Convergence was ensured by comparing the velocities in a 10-fold less dense grid, which resulted in less than 0.1% deviations.

Table 1. Variation of τ (Defined by Eq 1) and Measured Nonretained Minimal Plate Height and Corresponding Optimal Linear Velocity for the Different Considered Aspect Ratio (AR) REP Columns

aspect ratio	τ	$H_{x,\min}$ (μm)	$u_{x,\mathrm{opt}}$ (mms/s)
AR = 9	4.425	0.57	0.59
AR = 12	5.669	0.42	0.47
AR = 15	6.916	0.32	0.37
AR = 20	8.995	0.25	0.29

DOI: 10.1021/acs.analchem.5b01579
Anal. Chem. XXXX, XXX, XXX−XXX

RESULTS

Figure 2 shows CCD camera images of the rapid separation of 4 coumarin dyes separated using the retentive effect of a

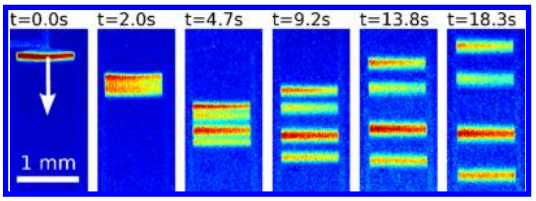

Figure 2. CCD Separation of 4 components within the first few millimeters of a REP column with width = 1 mm and filled with REPs with AR = 15 (velocity of nonretained mobile phase: u_x = 0.32 mm/s). Timing as indicated on figure (camera at rest in first 3 images and moving to keep the components in the middle of the image in the last 3 panels). Mobile phase composition: 65%/35% w/w water/methanol.

monolayer of octylsilane (C8) coated on the outer surface of the pillars. As can be noted, the 4 coumarin dyes rapidly separate in the first 3 mm of the REP column, reaching baseline separation resolution in some 5 to 10 s.

To measure the separation efficiency with the highest possible degree of accuracy, a maximum number of measurement points was collected both in time and space. Figure 3a shows the recording of the gradual band broadening process occurring during a typical experiment. The band clearly maintains its near-perfect Gaussian shape all along the 4 cm long trajectory.

Figure 3b shows how the variance of the band varies in a linear way with the elapsed distance. From the slope, it can be calculated that the band in the experiment shown in Figure 3a broadens at an extremely slow rate, corresponding to a plate height of only H_x = 0.24 μm. Because the variance of the axial width of the sample bands was subtracted from the final bandwidth, the initial sample volume does not influence the (inherent) performance. When the initial bandwidth (typically 100 μm) is not taken into account, the obtained efficiencies are influenced when the channel length is below 10 cm. For a nonretained component (C440 in methanol), the plate height increases, e.g., from H_x = 0.24 to 0.34 μm for a 4 cm channel but only up to a value of H_x = 0.25 μm for an 8 cm long channel.

In terms of number of theoretical plates, N, this corresponds to N = 160 000 theoretical plates (unretained analytes). For the AR = 15 column, the minimal H_x value for the nonretained component equaled 0.32 μm, which is significantly smaller than the H_x = 0.50 μm value obtained in ref 18, owing to the greater through-pore uniformity and higher resolution with which the presently investigated columns were fabricated.

To put the above values in perspective, it should be noted that the plate height in a packed bed of 5 μm-sized fully porous spheres (same diameter as the shortest diagonal of employed REPs) is of the order of some 10 μm and maybe some 5 μm if the spheres would be nonporous, which is at least an order of magnitude larger than measured here.

Figure 4 summarizes all measured efficiencies as a function of the time it took the band to leave the column. This type of plot is known as a fixed length kinetic plot[19] and was generated by applying different pressures to induce different velocities in each of the different AR columns. Considering Figure 4a, the separation efficiency that can be achieved in a given time in the 4 cm long channels clearly increases with increasing aspect

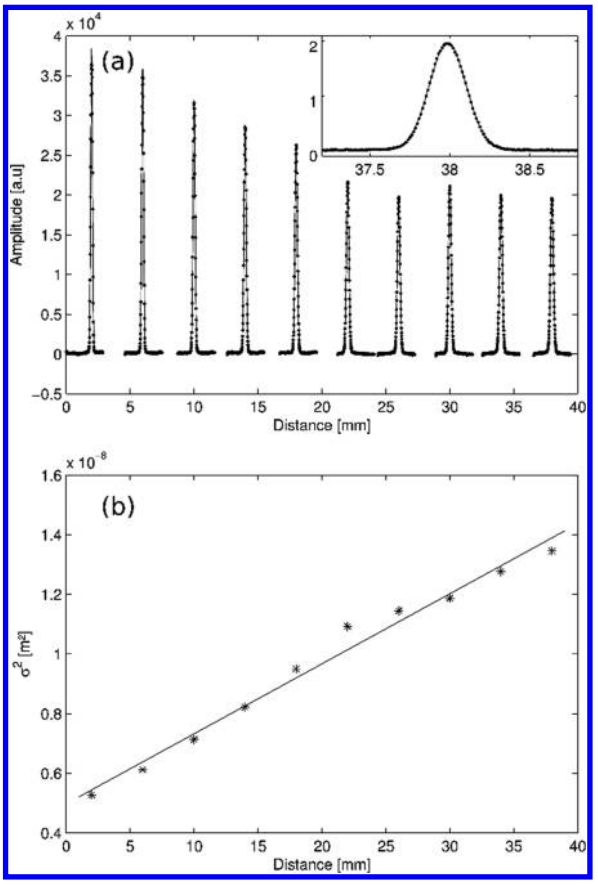

Figure 3. (a) Evolution of the concentration curve of an analyte band flowing through an AR = 20 column with a length of 40 mm, measured by moving a CCD camera to different positions (zoom-in shows Gaussian nature of bands, as well as high resolution of local concentration measurement recorded with a data point resolution of 0.009 mm); (b) corresponding evolution of the spatial variance of σ_x^2 as a function of the position x in the column. Slope of straight line relationship equals H_x = 0.235 μm.

ratio, with the maximally achievable N ranging from 70 000 (AR = 9) to 160 000 (AR = 20). This trend is less clear for the retained case (Figure 4b), where the increase of N with the AR can essentially only be clearly noted in the range of large times. In the short time range, the situation is more confusing because the retention factor k observed for a given mobile phase composition varied quite significantly between the different AR cases (see caption to Figure 4 for the actual k values). This variation was much larger than expected on the basis of the relatively small differences in available pillar surface (less than 1% difference between different AR columns). Therefore, its cause should be sought in accidental differences in the surface quality of the different columns or variations in the efficiency of the applied coating chemistry.

THEORY AND DISCUSSION

To interpret the results shown in Figure 4, it is helpful to first consider the following two different coordinate systems. One is the traditional x-coordinate (running along the mean flow direction; see x-arrow in Figure 1a), while the other is oriented along the tortuous path of the interpillar pores (see tortuous i-arrow in Figure 1b). Introducing the subscript "x" and "i" to denote whether any of the considered quantities (N, length, velocity, plate height, and so on) is measured in x-coordinates

DOI: 10.1021/acs.analchem.5b01579
Anal. Chem. XXXX, XXX, XXX−XXX

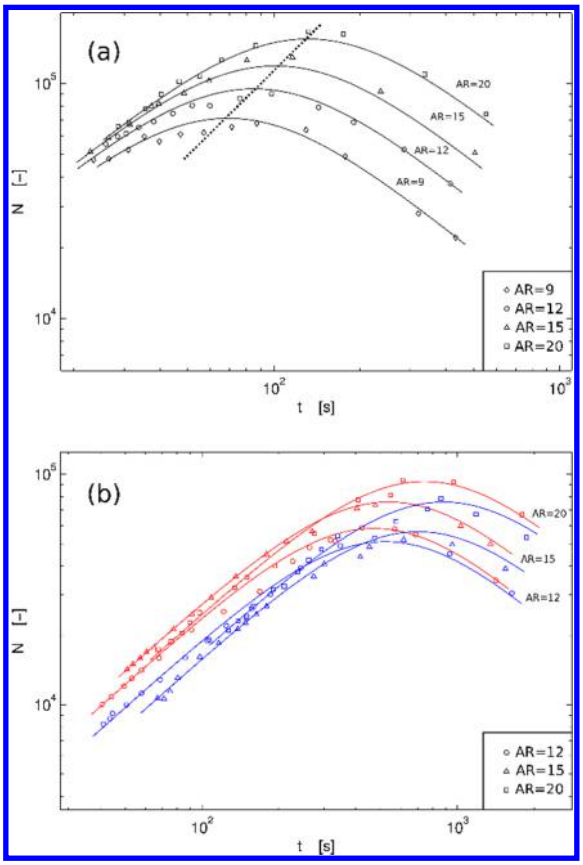

Figure 4. Curves of number of theoretical plates N vs (retained) time measured on the 4 cm long columns under (a) nonretained and (b) retained conditions. Red curves for mobile phase conditions of 65%/35% w/w water/methanol (leading to retention factors of k = 0.49 (AR = 12); k = 0.36 (AR = 15); k = 0.50 (AR = 20)). Blue curves for mobile phase conditions of 70%/30% w/w water/methanol (leading to retention factors of k = 1.03 (AR = 12); k = 0.80 (AR = 15); k = 1.12 (AR = 20)). The pressures corresponding to the performance maxima were in the range of 4−10 bar for nonretained components (100% methanol, $k' = 0$) and 1−3 bar for the retained components (70% water/30% methanol, $k' \sim 1$) for AR = 9 to AR = 20.

or in i-coordinates, the tortuosity parameter τ emerges as the natural parameter linking the elapsed distance and the average velocities in the different coordinate-systems:

$$\tau \equiv \frac{u_i}{u_x} = \frac{L_i}{L_x} \tag{1}$$

The internal reference frame (i-coordinate) is needed to describe the intrinsic band broadening, and the external frame (x-coordinate) is needed to describe how the quality of the separation is observed externally.

Link between N, t_R, and ΔP as Observed in the i- and x-Coordinate System. In a first instance, it is important to show that the considered performance parameters (number of theoretical plates, time, and pressure drop) are the same in both coordinate systems. For this purpose, and considering that the spread of the species band (represented by its spatial bandwidth w or band variance σ^2) can be measured in either x- or i-coordinates, it is important to realize that the tortuosity effect also squeezes the width of the bands when observed in the x-coordinate system, such that the relation between the w and σ^2 values measured in either of the two coordinate systems is also determined by τ:

$$w_x = \frac{w_i}{\tau} \quad \text{and} \quad \sigma_x^{\,2} = \frac{\sigma_i^2}{\tau^2} \tag{2}$$

As a control, it also readily follows from eqs 1 and 2 that the time needed to pass through the column and the temporal width (in time units) of the peaks eluting from the column is independent of the selected coordinate system, as it should be.

$$t_r = t_0(1 + k') \quad \text{with} \quad t_0 = \frac{L_i}{u_i} = \frac{L_x}{u_x} \tag{3}$$

$$\sigma_t = \frac{\sigma_x}{u_x}(1 + k') = \frac{\sigma_i}{u_i}(1 + k') \tag{4}$$

Similarly, the above relations also readily imply that the generated number of theoretical plates is independent of the coordinate system in which it is measured (either in time-, i-, or x-coordinates), also as it should be. This also allows one to use the general notation N (without subscript) for the plate number:

$$N_x = \frac{L_x^{\,2}}{\sigma_x^{\,2}} = \frac{L_i^{\,2}}{\sigma_i^{\,2}} = N_i = \frac{t_r^{\,2}}{\sigma_t^{\,2}} = N_t = N \tag{5}$$

The plate height (defined as $H \equiv \sigma^2/L$) on the other hand is not an invariant and depends on the selected coordinate system, as can be readily deduced from eqs 1 and 2.

$$H_x \equiv \frac{\sigma_x^{\,2}}{L_x} = \frac{(\sigma_i/\tau)^2}{L_i/\tau} = \frac{\sigma_i^{\,2}}{L_i}\frac{1}{\tau} \equiv \frac{H_i}{\tau} \tag{6}$$

The fact that N is independent of the reference frame (eq 5) whereas H is not (eq 6) shows that the true performance measure in chromatography is N and not H.

Dependency of N, t, and ΔP on τ and Relation to Performance in an Open-Tubular Channel (OTC). To further understand the results shown in Figure 4, we can turn to the hypothesis formulated in the introduction that an observer following the fluid along the tortuous i-coordinate of a REP column will experience the same type of band broadening as in an open-tubular channel (OTC). Mathematically, this hypothesis can be expressed as

$$H_{i,\mathrm{REP}} = \mathrm{H}_{\mathrm{OTC}} \tag{7}$$

For an open-tubular column, it is a well-established fact that H can be calculated as the sum of a pure B-term contribution (purely diffusion-driven band broadening observed when the flow is stopped) and a pure C-term band broadening (resistance to mass transfer in the radial direction, dominant at high velocities), each depending on the local velocity u_i:

$$H_{\mathrm{OTC}} = \frac{B}{u_i} + Cu_i \tag{8}$$

In packed columns, including cylindrical pillar array columns, an extra, flow velocity independent contribution (so-called A-term) is observed.[9,13] Combining the above with eq 6, it follows that

$$H_{x,\mathrm{REP}} = \frac{H_{i,\mathrm{REP}}}{\tau} = \frac{B}{u_i\tau} + C\frac{u_i}{\tau} = \frac{B}{u_x\tau^2} + Cu_x \tag{9}$$

Equation 9 implies that, under the adopted hypothesis, the B-term band broadening observed in the x-direction in REP columns with different τ values should decrease with τ^2, while the C-term contribution should remain unaltered (no τ-

DOI: 10.1021/acs.analchem.5b01579
Anal. Chem. XXXX, XXX, XXX−XXX

dependency). Interestingly, the proportionality constant (C) is the same in x- and in i-coordinates. The strong decrease of the B-term band broadening with increasing τ values obviously reflects the strong obstruction to longitudinal diffusion imposed by the REPs.

Taking eq 9 and using the general expressions for N ($= N_x = L_x/H_x$) and t_0 ($= L_x/u_x$), the following general relation between N_x and t_0 can be established:

$$N/\tau = \frac{t_0/\tau}{\frac{B}{{L_x}^2}\left(\frac{t_0}{\tau}\right)^2 + C} \tag{10}$$

Equation 10 implies that a plot of N/τ versus t_0/τ should yield coinciding curves when comparing REPs with the same linear length L_x but having different τ values. As can be noted from Figure 5a, where the N and t_0 values from Figure 4a are replotted, the experimental nonretained measurement data for the different τ-cases indeed nicely collapse onto one single curve, thus confirming the hypothesis underlying eq 7. The agreement is not as good for the cases with the smallest AR and then becomes better for the two largest aspect ratio cases. This is in agreement with the fact that the relative contribution of the turns, where the flow deviates from the pure parabolic open-channel flow marking the rest of the pillar array (cf. Figure 1b), is reduced with increasing aspect ratio. The data overlap slightly less well for the retained component cases (Figure 5b), due to the slight differences in retention factor k between the columns with different AR values but the same mobile phase composition (consider curves with the same color), as already mentioned before (see caption to Figure 4 for actual k values). The fact that the data points can be so well fitted with eq 10, i.e., without the need for an A-term, shows that the system behaves as a pure open-tubular system, which is the only chromatographic system without A-term contribution. In a previous study with cylindrical pillars, A-term contributions as high as $h_A = 0.25$ to 0.45 times the pillar diameter were observed.[13]

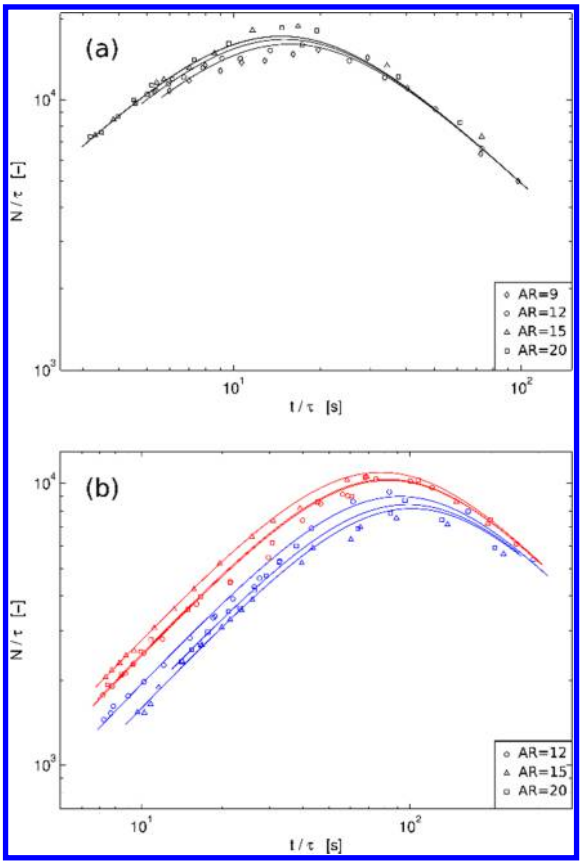

Figure 5. Same data as Figure 4 but now normalized as N/τ vs t/τ. Fitting with eq 10.

Equation 10 in itself is not sufficient to make statements about the actually achievable separation speed, because whether or not a given N or t can be achieved depends on whether or not the system can deliver the required pressure ΔP. The latter can most conveniently be expressed as a function of the local velocity u_i using Darcy's permeability law:

$$\Delta P = \frac{u_i \eta L_i}{K_{vi}} \tag{11}$$

wherein K_{vi} is the permeability of an OTC with a flat-rectangular cross-section, for which it is, from Poiseuille's law, well-known that $K_{vi} = d^2/12$ (d = width of channel for OTCs; d = distance between pillars for REP columns).

Combining eqs 10 and 11 to compare the effect of τ on the separation speed, the outcome will depend on the selected column length and velocity as both appear as a variable in eq 11. Table 2 summarizes the effect of τ on the expected kinetic performance for four of the most relevant combinations of column length and velocity. The comparison is made for two different column length cases, one wherein the linear length is the same (same L_x for all τ) and one in which the internal path length is the same (same L_i for all τ). For the velocity, it is straightforward to compare either for the same through-pore velocity (same u_i for all τ) or for the same net linear velocity (same u_x for all τ). The derivation of the relations summarized in Table 2 is given in the Supporting Information.

Table 2. Effect of τ on Kinetic Performance for Various Comparison Modes (=Combinations of Length and Velocity)

	same L_x	same L_i
same u_i	$t \sim \tau$	t = constant
	$\Delta P \sim \tau$	ΔP = constant
	$N \sim \tau$	N = constant
same u_x	t = constant	$t \sim 1/\tau$
	$\Delta P \sim \tau^2$	$\Delta P \sim \tau$
	N = constant (high u_x)	$N \sim 1/\tau$ (high u_x)
	$N \sim \tau$ (optimal u_x)	N = constant (optimal u_x)
	$N \sim \tau^2$ (low u_x)	$N \sim \tau$ (low u_x)

The main conclusion from Table 2 is that, as long as ΔP is not a limiting factor, i.e., as long as an increase of ΔP with τ is not a problem, the use of REPs with increasing τ can lead either to an increase of N for the same time or to a decrease of the time while maintaining N (cf. the cases for constant u_x, at the bottom row of Table 2). In the practically most important range of operating velocities, i.e., around the optimum u_x–velocity, this gain can be very significant: τ times more plates with REP than with OTC in the same time or τ times faster analysis with REP than with OTC while still producing the same N (2nd entry on bottom row of Table 2). Considering that τ can easily amount up to 10, this gain is indeed highly substantial. The advantage is even larger ($\sim\tau^2$) for lower

DOI: 10.1021/acs.analchem.5b01579
Anal. Chem. XXXX, XXX, XXX−XXX

velocities (*B*-term dominated), while at high velocities the advantage of a high τ disappears.

Table 2 also shows that these gains require an increase of the operating pressure according to either τ or even τ^2. In practice, this pressure margin is indeed available. Mass loadability typically limits the diameter of OTCs to some 5 μm and current affordable etching limitations (using mid-UV photlitography) do not allow one to bring the pillars in a REP column closer than about 2.5 μm. For the present REP, the pressure drop needed to produce 100 000 theoretical plates under retained conditions (extrapolated from the present column producing 70 000 plates) is only of the order of about 5 bar for AR = 20. Given that commercial liquid chromatography instruments these days can operate at pressures up to 1500 bar, the margin for a pressure increase is considerable. Since reducing the internal sizes of the columns seems to be very difficult, for either mass loadability reasons (OTC) or machining resolution (REP columns), increasing ΔP by building chromatographic systems with a high τ seems the most viable option with the current state of technology.

Whereas the above gains are obtained by comparisons of the same u_x—velocity, comparing for the same u_i while allowing for the same linear length L_x (1st entry on top row of Table 2), a τ-fold increase in N can be obtained as well, but in this case, this is realized at the expense of a τ-fold increase of the analysis time, as well as a τ-fold increase of the pressure drop. When ΔP is limiting and hence not allowed to further increase with increasing τ, both u_i and L_i need to be kept constant, which in the latter case implies that the linear length needs to be decreased according to $L_x \sim 1/\tau$. In this case, the advantageous effect of a large τ can no longer be exploited and each system simply produces the same N in the same time (2nd entry on top row of Table 2). The REP column then simply behaves as a folded OTC, producing exactly the same N in the same time as a normal, i.e., nonfolded OTC, but just requiring a shorter length L_x.

Besides the possibility to increase the speed or the efficiency (albeit at the expense of an increased pressure), REP columns have another, more general advantage over OTCs. Because a REP column offers a multitude of parallel paths, whereas a conventional OTC by definition has only one, REP columns can separate larger sample volumes and masses than OTCs. This is important, because mass loadability is precisely the Achilles' heel of OTCs. The reason why REP columns can offer a multitude of parallel paths, whereas this is not possible with conventional OTCs, is the presence of regular connection points between the different flow paths in a REP column. These allow for regular remixing between adjacent flow paths. This remixing is needed to overcome the so-called polydispersity problem, which puts a fundamental upper limit on the number of theoretical plates that can be achieved in a parallel array of nonconnecting OTCs as described by Schisla et al.[20] This polydispersity problem originates from the fact that even a small difference in permeability between two adjacent but noncontacting flows prevents N from increasing above a certain value. A small 1% difference in permeability (corresponding to a 0.5% precision in channel width) is already enough to limit the achievable number of plates to N = 10 000 no matter how long the column or small the channel width.[21] Aiming at columns producing 100 000 to 1 million theoretical pates, channel width accuracies in the order of 0.05% would be needed. Such accuracies are impossible to achieve in practice, not even with the most advanced micromachining technology. We experienced this effect when trying to put the REPs closer together (1.5 and 2 μm interpillar distance instead of the currently reported 2.5 μm) and witnessed an increase in plate height instead of a decrease. This also implies that machining precision imposes a practical upper limit for the tortuosity factor, because a large τ also means a reduction of the connection points, and these are needed for the re-equilibration of the flow between adjacent channels.

Studying Table 2 more in depth for the case considered in Figure 4, i.e., for the case of the same L_x and same u_x (1st entry on bottom row of Table 2), eq (S5) of the Supporting Information predicts that the effect of τ vanishes at high velocities and that REPs with different τ can all be expected to produce the same efficiency in the same time, equal to that of a straight OTC. This is indeed what is observed experimentally in Figure 4a, where the curves in the small t_0 range clearly converge to each other.

On the other side of the velocity scale (very small velocities leading to large t_0 times), eq (S6) of the Supporting Information shows that it should be possible to increase N in proportion with τ^2, while keeping the same analysis time. This behavior is indeed also observed in practice, as can be inferred from the distance between the N and t curves on the right-hand side of Figure 4 (large t_0 range).

Given the two velocity extremes display a strongly different dependency on τ, it can be expected that the gain in efficiency in the range of intermediate velocities will lie somewhere between both extremes. This is indeed the case, as can readily be verified from Figure 4, which is in full agreement with eq (S8) of the Supporting Information. Equation (S8) of the Supporting Information shows that a linear gain in efficiency can be expected when operating near the optimal velocity, i.e., the velocity for which the number of theoretical plates becomes maximal. The dashed line added to Figure 4a shows that the experimental data points indeed follow the law predicted by eq (S8) of the Supporting Information. For the retained cases (Figure 4b), there are some deviations, mainly because, as already mentioned, the retention factor that resulted from our coating procedures is somewhat dissimilar for the different AR cases.

As a next step in this study, it is planned to cover the pillars with a thick mesoporous layer via either electrochemical anodization or sol—gel deposition to provide a higher retention surface. This was not done at the present stage, to avoid that differences in layer quality between the different columns would obscure the τ-effect.

CONCLUSIONS

The intrinsic chromatographic band broadening prevailing in the tortuous paths meandering between the micropillars in microfabricated packed bed columns with radially elongated pillars (REPs) is identical to that experienced in the open-tubular column (OTC). This is an important advantage because OTCs are known to have much better speed and efficiency characteristics than conventional packed bed columns. Moreover, whereas OTCs are impractical to use because they only consist of a single micrometer sized channel and hence have a limited mass loadability, packed bed REP columns combine a multitude of parallel separation paths, thus offering a much larger mass loadability.

Conducting chromatographic experiments on 4 cm long micromachined packed bed columns filled with radially elongated pillars, separation efficiencies corresponding to N =

DOI: 10.1021/acs.analchem.5b01579
Anal. Chem. XXXX, XXX, XXX−XXX

160 000 theoretical plates (unretained analytes) and N = 80 000 theoretical plates were achieved, despite the relatively large interpillar distance (2.5 μm). In a bed packed with spherical 5 μm particles, a column length of 80 cm would typically be needed to achieve such efficiencies.

Comparing REP columns and OTCs under conditions of equal pressure drop, both systems can be expected to produce the same efficiency N in the same time. The REP column then simply behaves as a parallel array of folded OTCs, producing exactly the same N in the same time as a normal, i.e., nonfolded OTC, but just requiring a shorter linear length L_x.

However, when the pressure drop is not limiting, REP columns can significantly outperform OTCs in terms of the time needed to achieve a given N or the efficiency that can be achieved for a given time. This gain can be very significant. Around the optimal velocity, either the separation efficiency can be increased approximately linearly with the bed tortuosity τ ($N \sim \tau$) for the same time or the time can be reduced $\sim 1/\tau$ while N stays the same. Considering furthermore that τ values can easily be as high as 10, the large advantage of REP columns under nonpressure drop limited conditions is obvious. To the best of our knowledge, it is the first time this potential is highlighted.

It is important to realize that these gains can only be achieved at the expense of a higher pressure. This needs to be raised in proportion to either τ or τ^2, depending on the considered comparison (cf. bottom row of Table 2). For REP columns and OTCs, this pressure increase margin is available, because machining limitations and mass loadability concerns force the use of relatively large channel widths, inducing only small pressure drops.

■ ASSOCIATED CONTENT

Supporting Information

Additional information as noted in text. The Supporting Information is available free of charge on the ACS Publications website at DOI: 10.1021/acs.analchem.5b01579.

■ AUTHOR INFORMATION

Corresponding Author

*E-mail: wdemalsc@vub.ac.be. Phone: +32 2 629 37 81.

Notes

The authors declare the following competing financial interest(s): Gert Desmet and Wim De Malsche hold shares of the spin-off company PharmaFluidics that has been founded to commercialize micropillar array columns.

■ REFERENCES

(1) Horie, K.; Sato, Y.; Kimura, T.; Nakamura, T.; Ishihama, Y.; Oda, Y.; Ikegami, T.; Tanaka, N. *J. Chromatogr. A* **2012**, *1228*, 283−291.
(2) Pevzner, P.; Smith, R. D.; Heffron, F.; Adkins, J. N.; Paša-Tolic, L. *Proc. Natl. Acad. Sci. U.S.A.* **2013**, *110*, 10153−10158.
(3) Shen, Y.; Zhang, R.; Moore, R. J.; Kim, J.; Metz, T. O.; Hixson, K. K.; Zhao, R.; Livesay, E. A.; Udseth, H. R.; Smith, R. D. *Anal. Chem.* **2005**, *77*, 3090−3100.
(4) Zheng, S.; Ross, E.; Legg, M. A.; Wirth, M. J. *J. Am. Chem. Soc.* **2006**, *28*, 9016−9017.
(5) Ansong, C.; Wu, S.; Meng, D.; Liu, X.; Brewer, H. M.; Deatherage Kaiser, B. L.; Nakayasu, E. S.; Cort, J. R.; Pevzner, P.; Smith, R. D.; Heffron, F.; Adkins, J. N.; Pasa-Tolic, L. *Proc. Natl. Acad. Sci. U.S.A.* **2013**, *110*, 10153−10158.
(6) Alley, W. R.; Mann, B. F.; Novotny, M. V. *Chem. Rev.* **2013**, *113*, 2668−2732.
(7) Kennedy, R. T.; Oates, M. D.; Cooper, B. R.; Nickerson, B.; Jorgenson, J. W. *Science* **1989**, *246*, 57−63.
(8) Guiochon, G. *Anal. Chem.* **1981**, *53*, 1318−1325.
(9) Poole, C. F.; Poole, S. K. *Chromatography Today*; Elsevier: Amsterdam, 2012; pp 1037.
(10) Wang, D.; Hincapie, M.; Rejtar, T.; Karger, B. L. *Anal. Chem.* **2011**, *83*, 2029−2037.
(11) Collins, D. A.; Nesterenko, E. P.; Brabazon, D.; Paull, B. *Anal. Chem.* **2012**, *84*, 3465−3472.
(12) Singhal, R.; Mochalin, V. N.; Lukatskaya, M. R.; Friedman, G.; Gogotsi, Y. *Sci. Rep.* **2012**, *2* (510), 1−6.
(13) De Malsche, W.; Eghbali, H.; Clicq, D.; Vangelooven, J.; Gardeniers, H.; Desmet, G. *Anal. Chem.* **2007**, *79*, 5915−5926.
(14) Aoyama, C.; Saeki, A.; Noguchi, M.; Shirasaki, Y.; Shoji, S.; Funatsu, T.; Mizuno, J.; Tsunoda, M. *Anal. Chem.* **2010**, *82*, 1420−1426.
(15) Taylor, L. C.; Lavrik, N. V.; Sepaniak, M. J. *Anal. Chem.* **2010**, *82*, 9549−9556.
(16) He, B.; Tait, N.; Regnier, F. E. *Anal. Chem.* **1998**, *70*, 3790−3797.
(17) Op De Beeck, J.; Callewaert, M.; Ottevaere, H.; Gardeniers, H.; Desmet, G.; De Malsche, W. *Anal. Chem.* **2013**, *85*, 5207−5212.
(18) De Malsche, W.; Op De Beeck, J.; De Bruyne, S.; Gardeniers, H.; Desmet, G. *Anal. Chem.* **2012**, *84*, 1214−1219.
(19) Broeckhoven, K.; Desmet, G. *TrAC* **2014**, *63*, 65−75.
(20) Schisla, D. K.; Ding, H.; Carr, P. W.; Cussler, E. L. *AIChE J.* **1993**, *39*, 946−953.
(21) Billen, J.; Desmet, G. *J. Chromatogr. A* **2007**, *1168*, 73−99.

DOI: 10.1021/acs.analchem.5b01579
Anal. Chem. XXXX, XXX, XXX−XXX